Multiphoton classification of prethreshold structures in measured microwave ionization curves of hydrogen Rydberg atoms

T. Clausen* and R. Blümel
Department of Physics, Wesleyan University, Middletown, Connecticut 06459-0155, USA
(Received 15 July 2003; published 23 November 2004)

We present a complete multiphoton classification of prethreshold structures in measured microwave ionization data of hydrogen Rydberg atoms. We show that fourth-order quasienergy perturbation theory reproduces the locations of prethreshold structures, thus proving that prethreshold structures are a perturbative effect. Additional prethreshold structures are predicted to occur at field and frequency values, to our knowledge, not yet explored experimentally.

DOI: 10.1103/PhysRevA.70.053411 PACS number(s): 32.80.Rm

I. INTRODUCTION

In the early 1970s Bayfield and Koch performed an experiment which is still regarded as one of the key experiments in quantum chaos: the ionization of hydrogen Rydberg atoms by strong, linearly polarized microwave fields [1]. The central result of this experiment is the existence of sharp ionization thresholds as a function of field strength which were shown theoretically to coincide with chaos thresholds [2–4]. Detailed follow-up experiments performed by Koch and his group at Stony Brook [5–7] revealed additional structures in measured ionization curves which occur before the main rise of the ionization signal. We refer to these structures as prethreshold structures. The explanation of their physical origin and their classification in terms of multiphoton transitions from the initial state n_0 to n_0+1 is the focus of this paper.

Hydrogen ionizes at field strengths 10–20 times higher than alkali atoms for microwave frequencies lower than the Kepler frequency [8–10]. The stability of hydrogen (due to the absence of an ionic core) means that hydrogen is stable at field strengths high enough to produce ionization via multiphoton resonances between n_0 to n_0+1 of order up to 18 and higher before the system is driven into classical chaos.

A series of broad resonances, where the microwave field is a subharmonic of the Kepler frequency, leading to increased stability of the atom, has been reported [5,6,11]. These resonances appear in experiments with both hydrogen and hydrogenlike Rydberg atoms. These resonances, however, are different from the multiphoton resonances that are the focus of the present paper. The resonances discussed in this paper are much narrower in frequency and lead to prethreshold structures. The presence of added stability due to "classical subharmonic resonances" [12] actually works in our favor. It helps to reveal the presence of prethreshold structure by pushing the main rise of the ionization curve to higher fields.

It has been known for a long time that the prethreshold structures are due to anticrossings of Floquet states [13,14]—i.e., multiphoton transitions. But the present paper is, to our knowledge, the first time that specific multiphoton orders giving rise to experimental prethreshold structures have been assigned explicitly. In addition, we show that the analytical description of the perturbed levels is well within the reach of perturbation theory.

Prethreshold structures have been reported in recent experiments [12,15]. Here we concentrate on the experiments performed by Koch at Stony Brook, since these experiments cover a wide range of initial main quantum numbers.

In the Stony Brook experiments hydrogen atoms are prepared in a state with principal quantum number n_0 with a microcanonical distribution in angular momentum (l) and magnetic substates (m). The atoms are then exposed to a linearly polarized microwave field of field strength $\mathcal{E}$ and fixed frequency f. The microwave frequency f depends on the geometry of the cavity used in the experiments, and experimental single-frequency ionization curves for $f=7.58$ GHz, 9.92 GHz, and 11.89 GHz have been reported [7]. Throughout this paper, we will focus on the $f=9.92$ GHz data. Following the microwave irradiation, the fraction P of ionized atoms is recorded as a function of the microwave field strength $\mathcal{E}$ resulting in an ionization curve $P(\mathcal{E})$. Since every experiment, including the Stony Brook experiments, has a finite energy resolution and the hydrogen atom has an accumulation point in its bounded spectrum at zero energy, it is clear that the Stony Brook experiments cannot separate between true ionization—i.e., excitation into the positive-energy continuum and excitation into extremely highly excited bounded states. Thus the experimentally reported ionization signal contains both true ionization and excitation into bounded states with principal quantum numbers $n>n_c\approx 90$ [6]. The technical term "ionization" (the word ionization in quotation marks) has been proposed to refer to this situation [6]. We do not use this term in this paper, since we believe that no confusion will arise. Whenever we refer to ionization in the experimental context, it is clear that "ionization" is meant. Whenever we refer to ionization in the theory context, we mean excitation into high-lying bounded states with $n>n_c$ since, as discussed below (see Sec. II), our computations do not include the positive energy continuum.

A typical measured ionization curve ($n_0=37$) is shown as the dashed line in Fig. 1 [16]. Both a prethreshold structure and the main rise of the ionization signal are clearly seen.

*Electronic address: tclausen@wesleyan.edu

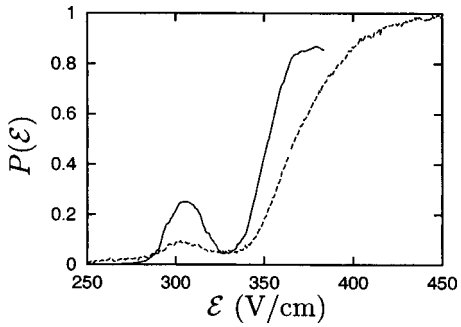

FIG. 1. Dashed line: experimental ionization probability of $n_0=37$ hydrogen Rydberg atoms exposed to ≈300 cycles of a linearly polarized microwave field of frequency 9.92 GHz as a function of field strength $\mathcal{E}$. Solid line: field-averaged ionization probability $\overline{P(\mathcal{E})}$ computed on the basis of the one-dimensional SSE model as discussed in the text.

Prethreshold structure is not an isolated phenomenon. This is illustrated in Fig. 2, which shows a gallery of measured ionization curves for $n_0=32,\ldots,50$ [16]. Figure 2 shows that prethreshold structure occurs in the ionization curves for $n_0=32,34,35,37,38,41,45,50$. These n_0 values are summarized in the first column of Table I. The prethreshold structures are marked by arrows in Fig. 2.

It is known that prethreshold structures are caused by ac Stark-shifted multiphoton resonances [17]. We show below that it is possible to find the order of the relevant multiphoton resonances and that the locations of prethreshold structures can be explained and predicted on the basis of simple fourth-order perturbation theory.

Since the prethreshold structures occur before the onset of classical chaos, their investigation, naturally, never took center stage in the quantum chaos context. This fact notwithstanding, some theory has already been addressed at explaining their origin. For instance, the role of two-state resonances for weak-field conditions was discussed by Dhar *et al.* using an impulsive drive [18]. They find no evidence of chaotic behavior, suggesting that ionization is driven by the presence of resonances. Blümel and Smilansky showed [19,20] that the prethreshold structures result from quasienergy anticrossings leading to probability transfer to higher-lying states which ionize easily. Richards *et al.* [7,21] were able to identify multiphoton resonances between two adiabatic states as responsible for the presence of prethreshold structures but did not assign multiphoton orders to experimentally measured prethreshold structures. Our treatment is complementary to the one presented by Richards *et al.* [7,21] as it aims at explaining the structures present in experimental data and

TABLE I. Properties of the prethreshold structures in published microwave ionization curves [5–7]. First column: principal quantum number n_0 of initially prepared state whose ionization curve shows prethreshold structure. Second column: multiphoton order ν assigned to the prethreshold structure in the n_0-ionization curve. Third column: field strength $\mathcal{E}_x$ where in our SSE calculations an anticrossing between the ac Stark-shifted states $|n_0\rangle$ and $|n_0+1\rangle$ ($n_0=32$, 34, 35, 37, 38, 41, 50) and $|n_0\rangle$ and $|n_0+2\rangle$ ($n_0=45$) occurs. Fourth column: smallest microwave field $\mathcal{E}_{cr}$ where in our classical SSE calculations at least one trajectory with initial classical action n_0 can reach $n>n_c=90$.

n_0	ν	$\mathcal{E}_x$ (V/cm)	$\mathcal{E}_{cr}$ (V/cm)
32	18	585	584
34	15	460	450
35	14	382	394
37	12	289	299
38	11	268	271
41	9	167	184
45	13	122	122
50	5	62	68

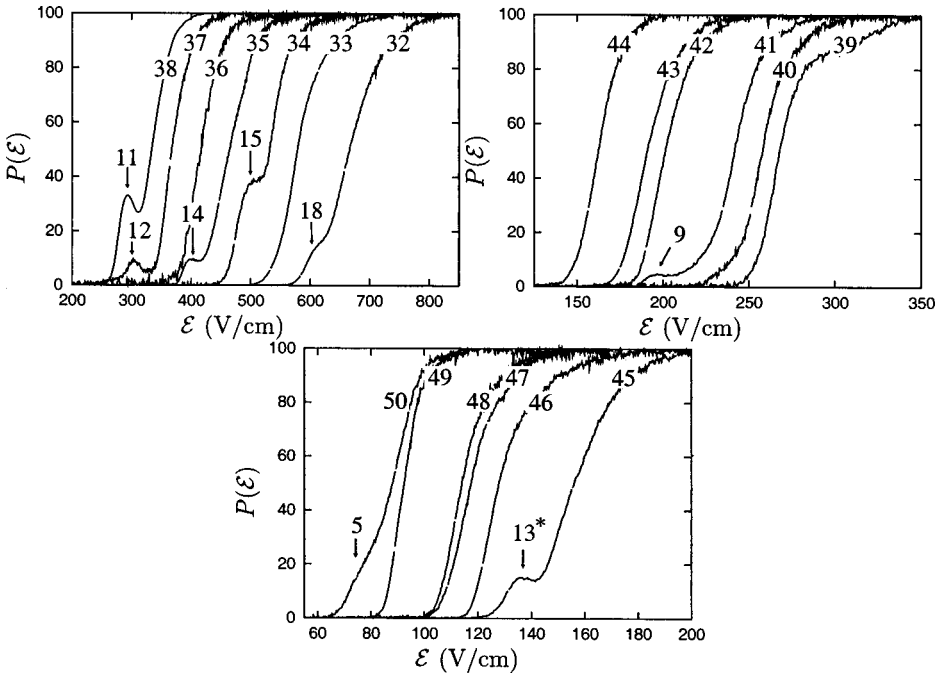

FIG. 2. Experimental ionization probabilities $P(\mathcal{E})$ [6,16] as a function of microwave field amplitude $\mathcal{E}$ at 9.92 GHz. The curves are labeled by their initial principal quantum numbers n_0. (a) $n_0=32,\ldots,38$, (b) $n_0=39,\ldots,44$, and (c) $n_0=45,\ldots,50$. Prethreshold structures are marked with arrows and labeled with their corresponding multiphoton orders ν. The multiphoton order $\nu=13$ in (c) is marked by a star since it corresponds to a transition from $n_0=45$ to $n=47$.

connects to the results of Blümel and Smilansky [19,20] via the picture of quasienergy anticrossings.

Our material is organized in the following way. In Sec. II we motivate, define, and justify the one-dimensional model we use to describe the quantum mechanical ionization process. In Sec. III we link prethreshold structures with multiphoton resonances and present our method for assigning multiphoton orders. In Sec. IV we introduce the concept of quasienergies and connect prethreshold structures with quasienergy anticrossings. In Sec. V we derive second- and fourth-order perturbation theory results for the ac Stark shift of atomic levels under the influence of a microwave field. We use these results to show that fourth-order perturbation theory is accurate enough to explain qualitatively and quantitatively the presence (or absence) of prethreshold structure in the measured ionization curves. In Sec. VI we discuss our results. Section VII concludes the paper.

II. MODEL

In recent years computers have become powerful enough to attempt complete three-dimensional calculations of microwave-driven hydrogen Rydberg atoms. Using a complex rotation approach, Buchleitner and co-workers have performed full three-dimensional calculations of alkali Rydberg atoms in a microwave field [9,10,22,23]. Yet when it comes to the extraction of the physical processes underlying a particular measured phenomenon, the most realistic calculations are not necessarily the best venue for attaining an enhanced understanding, since the core physical phenomenon may well be masked by a multitude of secondary processes completely taken into account by a full three-dimensional (3D) calculation. Therefore our goal is to select the simplest possible model that nevertheless retains the core physics of the phenomenon under investigation. Still, the calculations reported here took several months of runtime on a dedicated 90-node Beowulf cluster [24].

It has been known for a long time that the ionization dynamics of microwave-driven hydrogen Rydberg atoms is well described both qualitatively and to a certain extent even quantitatively by a one-dimensional model, the surface-state electron (SSE) model [25]. Within this model the Hamiltonian of the Rydberg electron (in atomic units) is given by

$$\hat{H}(z,t) = \hat{H}_0 + \varepsilon z \sin(\omega t), \quad \hat{H}_0 = \frac{1}{2}\hat{p}^2 - \frac{1}{z}, \tag{1}$$

where $\hat{p} = -i\partial/\partial z$ is the momentum operator, z is the spatial coordinate, t is time, and ε and ω are the microwave field strength and the microwave frequency, respectively. ϵ and ω in Eq. (1), and throughout this paper, are in atomic units. Frequently, in particular when we compare our results to the experimental data, it is more natural to refer to the field in V/cm and to the frequency in GHz. We then use the symbols $\mathcal{E}$ and f, respectively.

The model Hamiltonian (1) is the result of numerous simplifications, which, however, can all be justified. The most serious approximations are the following. (i) In realistic microwave ionization experiments [6] the Rydberg atoms enter a cavity which, in the reference frame of the atom, ramps the microwave field from zero to its peak value and then, upon leaving the cavity, switches the field off again. For the range of principal quantum numbers of interest here ($n_0 = 32, \ldots, 50$), the driving frequency of 9.92 GHz corresponds to an adiabatic situation in which the switch-on and switch-off of the microwave field can safely be neglected [13]. This is the reason why we do not include a time-dependent amplitude function in the drive term of Eq. (1). (ii) The Rydberg atoms enter the cavity at different times, effectively resulting in the presence of a random phase shift in the argument of the sin function in Eq. (1). In the experiments, because of the adiabatic switching of the field and the exposure of the atoms to hundreds of microwave field cycles, the random phase in the drive term has no effect on the measured ionization probabilities. Therefore, we set the phase to zero in Eq. (1). This also guarantees that the field starts with zero amplitude at $t = 0$. (iii) The velocity spread of atoms in the beam of hydrogen Rydberg atoms of $\Delta v/v \approx 7 \times 10^{-4}$ [7] corresponds to an uncertainty in the microwave exposure time of ≈ 0.2 cycles. This effect is negligible. (iv) It is known [26] that ionization curves depend critically on all three quantum numbers n_0, l_0, and m_0 of the initially prepared state of the Rydberg electron. In particular there is a strong dependence on m_0 [26]. There is no m dependence in the model Hamiltonian (1). However, the model Hamiltonian (1) closely models the hydrogenic $m = 0$ extremal Stark states which are known to ionize most efficiently in a linearly polarized field. Since the $m_0 = 0$ state is present in the initial microcanonical ensemble of the experimentally prepared states, our model describes at least some part of the initially prepared experimental state to a very good approximation. Since this is also the part of the initial state which ionizes first (in field) and most efficiently, we should be prepared to see ionization curves computed on the basis of Eq. (1) to be shifted slightly to the left as compared with experimental ionization curves, and the prethreshold structures are expected to be more pronounced.

Even the simple model (1) is still too complicated to be treated exactly. The most serious complication stems from the fact that $\hat{H}_0$ possesses a continuous spectrum. While methods exist to take the continuum into account [19,22], their implementation turns out to be too expensive for our present purpose. But since, as explained in the Introduction, existing experiments [6] do not separate between true ionization and excitation beyond n_c and since, in addition, not much is known about the branching ratio of electrons ending up in the true continuum and electrons ending up in highly excited states with $n > n_c$, we neglect the coupling to the $\hat{H}_0$ continuum and use excitation beyond n_c as a probe for the total experimentally measured ionization probability.

Based on the above discussion we implemented the following numerical procedure for solving numerically the quantum dynamics of a Rydberg electron governed by the Hamiltonian (1). We expanded the electron wave function in the set of 76 bounded $\hat{H}_0$ eigenstates with principal quantum numbers $n = 25, \ldots, 100$. This way the solution of the Schrödinger equation with the Hamiltonian (1) is turned into a system of 152 real, coupled, linear, first-order differential equations for the expansion coefficients. These coupled equations are propagated forward in time using an eighth-

order Runge-Kutta integrator method with variable step size [27]. An absorbing boundary condition at $n_c=90$ keeps track of the electron flux that reaches high-lying Rydberg states. The absorbing boundary condition is implemented in the following way: After each microwave cycle—say, cycle number j—the total occupation probability of the states with $n=91,\ldots,100$ is recorded as p_j. Then the amplitudes of states $n=91,\ldots,100$ are set to zero and cycle number $j+1$ is started. The total ionization probability is then computed via $P(\mathcal{E})=\Sigma_{j=1}^{N}p_j$, where $N=50$ is the total number of microwave cycles in our computations. This approach effectively models ionization due to phase-space diffusion [3]. In addition it greatly reduces spurious reflection of probability from the end of our truncated basis.

We used the above numerical method to compute the ionization curve for $n_0=37$ and $f=9.92$ GHz. For a better comparison with experiment we averaged $P(\mathcal{E})$ over the experimental field uncertainty of $\approx 7\%$ of peak field strength which results from the size of the entry aperture of the microwave cavity in conjunction with the spatial electric field distribution of the 9.92 GHz cavity mode [6]. The field-averaged $P(\mathcal{E})$ is shown as the solid line in Fig. 1. We see that Eq. (1) qualitatively reproduces the prethreshold structure and the main rise. As expected, the height of the prethreshold structure is overemphasized and the main rise of the ionization curve is slightly shifted to the left as compared with the experimental result (dashed line in Fig. 1). But most importantly Fig. 1 shows that both the position of the prethreshold structure and the onset of the main rise of the ionization curve are modeled by the Hamiltonian (1) to a good approximation. This is important since we base our interpretation of the prethreshold structures, including our multiphoton classification scheme and the position of the prethreshold structures, on the one-dimensional model. On the basis of Fig. 1 and many similar ionization curves that we computed, we conclude that the one-dimensional model (1) together with its numerical implementation is indeed a sound basis for the investigation of the physical mechanisms underlying the experimentally measured prethreshold structures.

III. PHYSICAL ORIGIN OF PRETHRESHOLD STRUCTURE

Since the prethreshold structures occur at relatively weak microwave field strengths below the main rise of the ionization signal, we expect that the low-lying energy levels of the atomic system in the prethreshold region are relatively well-defined ac Stark-shifted energy levels which are broadened considerably only for field strengths at or above the field strengths corresponding to the main rise of the ionization signal. Therefore we expect that the microwave field is able to drive multiphoton resonances between low-lying ac Stark-shifted atomic states.

Figure 3 shows a 3D plot of the ionization probability as a function of frequency and field strength for $n_0=37$. The prethreshold structures are clearly seen as "tongues" stretching down from high field strengths to low field strengths. The tongues get narrower at lower field strengths and bend toward higher frequencies.

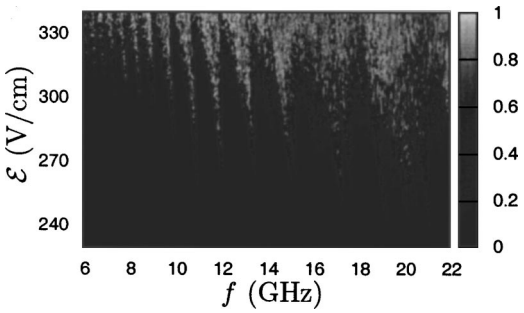

FIG. 3. False-color and gray-scale plot (see intensity scale to the right of the panel) of the ionization probability after 50 cycles as a function of frequency and field strength for $n_0=37$.

To identify the multiphoton order of a given prethreshold structure we use the following technique. For a given n_0 and frequency f we compute a complete ionization curve $P(n_0;\mathcal{E},f)$ as a function of field strength and identify the lowest field strength $\mathcal{E}_{10\%}(n_0;f)$ which results in 10% ionization probability after 50 cycles. Both the 10% level in the ionization probability and the microwave exposure of 50 cycles are chosen arbitrarily, but additional calculations showed that the method is not sensitive to these particular values. Then we create a data base of 10% field strengths for a dense grid of frequency values ranging from $f=6$ GHz to $f=22$ GHz in steps of 0.1 GHz. It turns out that these 10% field strengths lie approximately on a straight line $\mathcal{E}_{10\%}(n_0;f)\approx y(f)=\alpha(n_0)f+\beta(n_0)$, where, for $n_0=37$, e.g., $\alpha(37)=-3.97$ V/(cm GHz) and $\beta(37)=343$ V/cm. For low frequencies, the validity of this linear dependence is well established [6]. The motivation for the linear fit is the following. Locally, the fit averages out the presence of prethreshold structures and thus, on average, defines more accurately the onset of the main rise of the ionization signal.

We now define the fraction of ionization probability in the prethreshold region according to

$$P_<(n_0;f)=\int_0^{y(f)}P(n_0;\mathcal{E},f)d\mathcal{E}. \tag{2}$$

This quantity is a measure for the occurrence of prethreshold structure. If $P_<$ is small, there is no prethreshold structure. If $P_<$ is large, there is a pronounced prethreshold structure in the ionization signal. We should mention that in order to compute $P_<$, the linear fit procedure described above is not necessary. $P_<$ could just as well be computed by inspecting the individual ionization curves and determining the onset of the main rise visually. However, since we had to compute $P_<$ at thousands of frequency mesh points in order to establish our multiphoton interpretation and classification of prethreshold structures for all n_0 values in the range $n_0=32,\ldots,50$, this would have meant to examine literally thousands of ionization curves one by one. The linear fit, therefore, serves to automate the determination of the critical fields that mark the onset of the main rise.

Figure 4 shows $P_<$ computed for the complete frequency range from $f=6$ GHz to $f=22$ GHz for $n_0=37$. We see sharp resonances at well-defined frequencies. As shown in Fig. 4

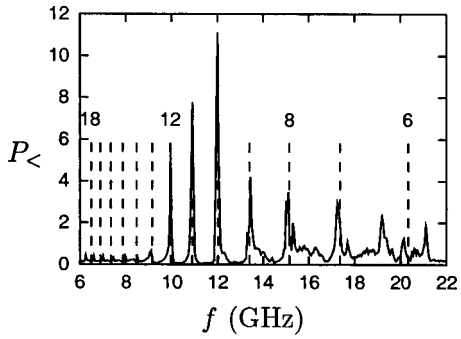

FIG. 4. Area $P_<$ under the ionization curve below the linear fit to the 10% ionization threshold as a function of frequency for $n_0=37$. The vertical dashed lines indicate the positions of multiphoton transitions from $n_0=37$ to $n=38$, shifted 0.45 GHz to the left. Selected peaks are labeled with their respective multiphoton orders.

the peaks in $P_<$ correlate exactly with the positions of multiphoton resonances between $n_0=37$ and $n_0=38$ if we reduce the energy spacing between $n_0=37$ and $n_0=38$ by 0.45 GHz to account for the ac Stark shift of both levels. The energy distance between $n_0=37$ and $n_0=38$ is reduced, because, as shown later (see Secs. IV and V), the ac field causes an attraction of levels. The shift is weakly frequency dependent (see Sec. V), with slightly more attraction for larger frequencies. This effect is counterbalanced by the fact that higher frequencies ionize at lower field strengths. Thus the overall effect is to render the shift at the position of the prethreshold structure virtually frequency independent.

As shown by Fig. 4 the spacing of the resonances in $P_<$ is completely regular such that a multiphoton order can be unambiguously assigned to each of the peaks. Since every peak in $P_<$ corresponds to a prethreshold structure and every peak in $P_<$ can be assigned a unique multiphoton order, there is a one-to-one correspondence between prethreshold structures and multiphoton transitions. Thus we proved that multiphoton resonances are well defined in the prethreshold regime and are the physical origin of the prethreshold structures. This result agrees with the earlier results by Richards *et al.* [7].

According to Fig. 4 the prethreshold structure in the $n_0=37$ ionization data is unambiguously identified as a 12-photon transition between the ac Stark-shifted states $n_0=37$ and $n=38$. In order to assign multiphoton labels to all the other prethreshold structures in the experimental ionization curves shown in Fig. 2, we computed $P_<(n_0;f)$ for each n_0 value in the range $n_0=32,\ldots,50$. On the basis of $P_<(n_0;f)$ it is then straightforward to assign the multiphoton order to a given prethreshold structure. For each n_0 showing prethreshold structure in the ionization curve (the first column in Table I), the second column in Table I shows the multiphoton order ν of the corresponding prethreshold structure. Thus we arrived at a complete multiphoton classification of measured prethreshold structures in the experimental $n_0=32,\ldots,50$, $f=9.92$ GHz ionization curves. Only the case $n_0=45$ is special because in this case the multiphoton transition is not between the initial state and the immediately neighboring state, but between $n_0=45$ and $n=47$. Still the multiphoton order is perfectly well defined and corresponds to a 13-photon transition.

IV. PRETHRESHOLD STRUCTURES AND QUASIENERGY ANTICROSSINGS

We now link prethreshold structures and quasienergy anticrossings. Since the microwave drive in Eq. (1) is periodic in time and the Schrödinger equation is linear, Floquet theory [28] is applicable. According to this theory the time-dependent Schrödinger equation

$$i\frac{\partial\psi(z,t)}{\partial t}=\hat{H}(z,t)\psi(z,t) \tag{3}$$

has solutions of the form

$$\Phi(z,t)=e^{-i\epsilon t}\phi(z,t), \tag{4}$$

where $\phi(z,t)=\phi(z,t+T)$, $T=2\pi/\omega$, is periodic in time and ϵ is called the *characteristic exponent* [29,30] or the quasienergy [31]. The method of quasienergies is closely related to the theory of Bloch waves in solid-state physics [32]. The terms "quasienergy states" and "ac Stark-shifted states" are physically the same; only the terminology is different.

Defining the one-cycle propagator $\hat{U}(T)$ that propagates the solutions of Eq. (3) over one cycle of the applied microwave field, we have

$$\Phi(z,T)=e^{-i\epsilon T}\phi(z,0)=\hat{U}(T)\Phi(z,0)=\hat{U}(T)\phi(z,0), \tag{5}$$

where we used the periodicity of ϕ. It follows immediately from Eq. (5) that the eigenvalues of $\hat{U}(T)$ are given by $\exp(-i\epsilon T)$. Therefore, the most convenient way to compute the quasienergies ϵ is to construct the one-cycle propagator and diagonalize it. Denoting by $\exp(i\alpha)$ the eigenvalues of $\hat{U}(T)$ and by $|\alpha\rangle$ the eigenstates of $\hat{U}(T)$,

$$\hat{U}(T)|\alpha\rangle=e^{i\alpha}|\alpha\rangle, \tag{6}$$

we have

$$\alpha=-\epsilon T \tag{7}$$

and

$$\langle z|\alpha\rangle=\phi(z,0). \tag{8}$$

We used this method to compute the quasienergy levels of our one-dimensional model for $n_0=37$ and $f=9.92$ GHz as a function of the microwave field strength $\mathcal{E}$. Since, based on the results of the previous section, the prethreshold structure in the $n_0=37$ ionization data is caused by a multiphoton transition between the ac Stark-shifted $n_0=37$ and $n=38$ states, we are mostly interested in the quasienergy states with the largest overlaps with the unperturbed $n_0=37$ and $n=38$ states. The resulting quasienergy states expressed as the eigenphases of $\hat{U}(T)$ according to Eq. (7), are shown as the solid lines in Fig. 5(a). At $\mathcal{E}=0$ they connect with the unperturbed eigenstates of $\hat{H}_0$. For increasing microwave field strength both states bend upwards and show an anticrossing at $\mathcal{E}=290$ V/cm which is precisely the location of the $n_0=37$ prethreshold structure. Thus we showed that the prethreshold structure in the $n_0=37$ data is due to a quasienergy anticrossing that occurs before the main rise (dashed vertical line in Fig. 5) of the ionization signal. As shown in Fig. 5(a),

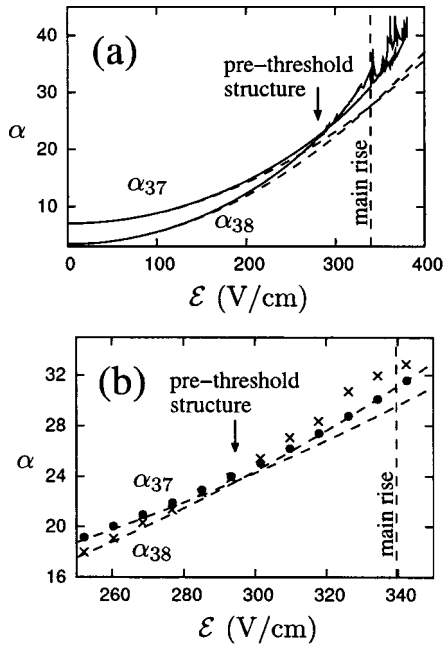

FIG. 5. Eigenphases α of the one-cycle propagator $\hat{U}(T)$ as a function of microwave field strength at $f=9.92$ GHz. Shown are the eigenphases α_{37} and α_{38} whose corresponding eigenstates $|\alpha_{37}\rangle$ and $|\alpha_{38}\rangle$ have the largest overlap with the unperturbed SSE states $|n=37\rangle$ and $|n=38\rangle$. The position of the prethreshold structure in the $n=37$ experimental ionization curve is marked by an arrow. The position of the onset of the main rise of the experimental ionization signal is marked by the vertical dashed line. (a) Solid lines: the numerically computed eigenphases α_{37} and α_{38}. They show an anticrossing at the position of the prethreshold structure. Dashed lines: the results for α_{37} and α_{38} obtained from second-order quasienergy perturbation theory. (b) Magnification of (a). The field mesh points do no longer blend into a continuous line and the corresponding results for α are shown as bullets (α_{37}) and crosses (α_{38}). For clarity of presentation only every third point is marked. Dashed lines: the results for α_{37} and α_{38} obtained from fourth-order quasienergy perturbation theory.

for still higher fields the quasienergy corresponding to the quasienergy state with predominantly $n=38$ character develops a jittery appearance, which is especially pronounced for fields in excess of the threshold field which marks the onset of the main rise of the ionization signal (dashed vertical lines in Fig. 5). This behavior is easily explained. At such high fields many quasienergy states with different quasienergies compete for the largest overlap with the $|n=38\rangle$ state. Thus the criterion of largest overlap results in the selection of structurally different quasienergy states whose different quasienergies are responsible for the observed jumps in Fig. 5.

In the same way we investigated all other prethreshold structures in the ionization data shown in Fig. 2. For each n_0 with prethreshold structure (first column in Table I) we were able to connect the prethreshold structure with a quasienergy anticrossing. The field strengths where the anticrossings occur are listed as the third column in Table I. They correlate remarkably well with the positions of the measured prethreshold structures in Fig. 2. Thus we established a one-to-one correspondence between quasienergy anticrossings and prethreshold structures.

V. PERTURBATION THEORY

As discussed above, prethreshold structures are due to multiphoton transitions between well-defined, ac Stark-shifted levels. In this section we show that energy levels computed using fourth-order quasienergy perturbation theory accurately predict the positions of prethreshold structures. Quasienergy perturbation theory is a well-known standard technique applicable to periodically driven quantum systems. Our implementation of the method closely follows the presentation in [33].

The Hamiltonian (1) has a periodic time dependence and can therefore be rewritten in time-independent form in a $(1+1)$-dimensional space Q, whose coordinates are z and t. The Hamiltonian $\hat{\mathcal{H}}$ acting in this space is given by

$$\hat{\mathcal{H}}(z,t) = \hat{H}(z,t) - i\frac{\partial}{\partial t}, \tag{9}$$

where $\hat{H}$ is the SSE Hamiltonian defined in Eq. (1). Due to the periodicity of the problem, the topology of Q is that of a cylinder. t is the cyclic coordinate where $t=0$ is identified with $t=T$. The eigenvalue problem for $\hat{\mathcal{H}}$ is given by

$$\hat{\mathcal{H}}(z,t)\phi_k(z,t) = \epsilon_k\phi_k(z,t), \tag{10}$$

where $\phi_k(z,t)$ are the T-periodic functions defined in Eq. (4). Setting

$$\hat{\mathcal{H}} = \hat{\mathcal{H}}_0 + \epsilon z\sin(\omega t) \tag{11}$$

leaves $\epsilon z\sin(\omega t)$ as a perturbation of the time-independent problem

$$\hat{\mathcal{H}}_0\phi_{nl} = E_{nl}^{(0)}\phi_{nl}, \tag{12}$$

where the inner product is defined as

$$\langle\phi_{nl}(z,t)|\phi_{n'l'}(z,t)\rangle_T = \frac{1}{T}\int_0^T \langle\phi_{nl}(z,t)|\phi_{n'l'}(z,t)\rangle dt. \tag{13}$$

The eigenvalues of Eq. (12) are $E_{nl}^{(0)}=-1/2n^2+l\omega$ and the eigenstates are $\phi_{nl}=e^{+i\omega l}|n\rangle$, where $|n\rangle$ are the eigenstates of $\hat{H}_0$ defined in Eq. (1).

The first- and third-order corrections due to the perturbation are zero. The second-order correction is

$$\Delta E_n^{(2)} = -\frac{1}{4}\sum_k z_{nk}^2\left(\frac{1}{E_n - E_k + \omega} + \frac{1}{E_n - E_k - \omega}\right), \tag{14}$$

where

$$z_{nk} = \langle n|z|k\rangle \tag{15}$$

is computed on the basis of the bound eigenstates $|n\rangle$ of $\hat{H}_0$ defined in Eq. (1). The fourth-order correction is

$$\Delta E_n^{(4)} = E_1\Delta E_n^{(2)} + E_2, \tag{16}$$

where

$$E_1 = -\frac{1}{4}\sum_{k\neq n} z_{nk}^2(\epsilon_{k,1}^2 + \epsilon_{k,-1}^2) \tag{17}$$

and

$$E_2 = \frac{1}{16}\sum_{k,l,m,\sigma_1,\sigma_2}\left(\frac{1}{2}\epsilon_{k,\sigma_1}\epsilon_{l,2\sigma_1}\epsilon_{m,\sigma_1} + \epsilon_{l,0}\epsilon_{k,\sigma_1}\epsilon_{m,\sigma_2}\right) z_{nk}z_{kl}z_{lm}z_{mn}. \tag{18}$$

We defined

$$\epsilon_{k,\sigma} = \frac{1}{E_n - E_k + \sigma\omega}, \tag{19}$$

and $\sigma_1 = \pm 1$, $\sigma_2 = \pm 1$, and $k,l,m = 1,\ldots,n-1,n+1,\ldots,M$, where $M = 100$ is our basis size. It is straightforward to prove analytically that Eq. (14) converges. We do not have an analytical proof for the convergence of Eq. (16), and therefore we do not know if the fourth-order perturbation correction actually converges. Numerically Eq. (16) is stable to within a relative error of $\approx 10^{-4}$ in bases up to 1000 SSE states.

The dashed lines in Fig. 5 show the result of second-order [Fig. 5(a)] and fourth-order [Fig. 5(b)] quasienergy perturbation theory for the $\hat{U}(T)$ eigenphases which connect with the eigenphases of the unperturbed states $|n_0 = 37\rangle$ and $|n = 38\rangle$ at zero field. We see that for small microwave field strengths the results of both second-order and fourth-order perturbation theory are very close to the numerically exact quasiphases. Both second and fourth order predict that for $n_0 = 37$ a quasienergy anticrossing occurs. But while second-order perturbation theory makes a qualitatively incorrect prediction by placing the anticrossing at the same field strength as the main rise, fourth-order perturbation theory makes the correct prediction that the anticrossing occurs *before* the main rise, resulting in a prethreshold structure. In fact fourth-order perturbation theory predicts the position of the anticrossing to within 5 V/cm, less than the width of the prethreshold structure itself. Thus we conclude that prethreshold structures are essentially a perturbative effect, well within the reach of fourth-order quasienergy perturbation theory.

VI. DISCUSSION

Our work is closely related to the work of Richards *et al.* [7] who investigate ionization curves in the adiabatic regime for principal quantum numbers ranging from $n_0 = 32$ to $n_0 = 48$. The main findings of Richards *et al.* are that (i) prethreshold structure is a low-frequency phenomenon, (ii) prethreshold structure in the adiabatic regime can be reproduced with as few as two (adiabatic) basis states, and (iii) classical calculations fail to reproduce the prethreshold structures, which are therefore a quantum phenomenon. We agree with the main findings of Richards *et al.* and add the following new aspects. (a) While Richards *et al.* work with adiabatic states, we find that Stark-shifted SSE states are also well suited for qualitative and quantitative calculations in the adiabatic regime. (b) In analogy to the result (ii) of Richards *et al.*, we find that two ac Stark-shifted states are sufficient to obtain the correct positions and multiphoton assignments of prethreshold structures. (c) We identify prethreshold structure as a multiphoton transition between two ac Stark-shifted states, usually the starting state n_0 and the first excited state n_0+1. (d) We arrive at a complete multiphoton classification of prethreshold structure including explicit assignments of multiphoton orders. (e) We show that perturbation theory is powerful enough to reproduce the positions of prethreshold structure quantitatively without any adjustable parameters.

In particular we agree with the authors of [7] that prethreshold structure is a low-frequency phenomenon. In our model the reason for this is obvious. We showed above that we obtain the most pronounced prethreshold structures for multiphoton transitions between n_0 and n_0+1. Expressed in scaled frequency $\omega_0 = \omega n_0^3$ [3]—i.e., the ratio of the microwave frequency and the Kepler frequency of the n_0th Bohr orbit—the distance between n_0 and n_0+1 is very close to $\omega_0 = 1$ for large n_0. Thus, n_0 and n_0+1 can be connected resonantly only for $\omega_0 \leqslant 1$. For $\omega_0 > 1$ the photon energy exceeds the level spacing between next nearest neighbors, and resonant transitions between n_0 and n_0+1 are no longer possible. What is, however, possible, at least for $\omega_0 < 2$, are transitions between n_0 and n_0+2. Indeed, as shown for the case $n_0 = 45$, such cases do occur. For $\omega_0 > 2$ even $n_0 \to n_0+2$ becomes impossible, but $n_0 \to n_0+\mu$, $\mu > 2$ is still possible. However, for $\mu > 2$, at typical prethreshold field strengths, these levels are very far in the continuum, such that a clear prethreshold structure is very hard, if not impossible, to achieve. These simple arguments show clearly that prethreshold structure is primarily a low-frequency phenomenon.

Figure 4 predicts prethreshold structures for $n_0 = 37$ for field and frequency combinations not yet explored experimentally. At $f = 12.0$ GHz, e.g., we predict a rather spectacular prethreshold structure. We confirmed the prediction of Fig. 4 by inspection of the computed $P(n_0 = 37; \mathcal{E}, f = 12.0\ \text{GHz})$ ionization curve.

For our numerical calculations we chose to look at the ionization probability after 50 cycles. The number of cycles, however, is not critical. Any number of cycles from about 30 to 300 (the experimental exposure time) yields the same results as far as the multiphoton assignments are concerned. We chose 50 cycles exposure time because it is a good compromise between accuracy of multiphoton assignment and economy of the calculations. After 50 cycles, most prethreshold structures are clearly identifiable while the signal is not saturated. The time scales of the main rise and the prethreshold structure are different, with the former showing up in only a few cycles while the prethreshold structure typically needs on the order or 15–20 cycles to manifest itself [19,20]. In a finite-basis-state calculation the detailed structure of the prethreshold structure is complicated, showing several narrow spikes [19,20] on a multitude of time scales [34]. This detailed structure, while interesting, is not relevant to the current analysis.

The problem of a limited basis size can be worked around by numerically studying the periodically kicked hydrogen Rydberg atoms. This allows for a detailed study of ionization dynamics in high-n states and accurate modeling of the probability distribution after long interaction times and in three

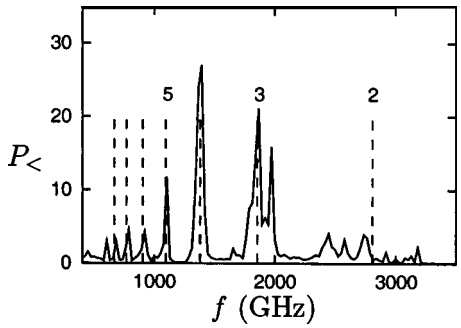

FIG. 6. Area $P_<$ under the ionization curve below the linear fit to the 10% ionization threshold as a function of frequency for $n_0=10$. Overlaid are the positions of multiphoton transitions from $n_0=10$ to $n=11$ shifted 0.45 GHz to the left. The photon order is noted above selected peaks.

dimensions [35–37]. Our aim here is to accurately model the positions of prethreshold structures and clearly separate the prethreshold structures from the main rise of the ionization signal. For this we found that a continuous drive model is absolutely necessary.

We found an interesting effect in the $f=9.92$ GHz data which deserves mentioning. Assume that there is a ν-photon transition from n_0 to n_0+1 and in addition, at the same field and frequency, a $(\nu-1)$-photon transition from n_0+1 to n_0+2. This results in the two conditions

$$\frac{1}{\omega}\left(-\frac{1}{2(n_0+1)^2}+\frac{1}{2n_0^2}\right)=\nu, \tag{20}$$

$$\frac{1}{\omega}\left(-\frac{1}{2(n_0+2)^2}+\frac{1}{2(n_0+1)^2}\right)=\nu-1, \tag{21}$$

from which, by subtraction, we obtain the following condition on the microwave frequency ω:

$$\frac{1}{2n_0^2}-\frac{2}{2(n_0+1)^2}+\frac{1}{2(n_0+2)^2}=\omega. \tag{22}$$

This is an interesting criterion since the left-hand side of Eq. (22) turns out to be approximately equal to the negative of the second derivative of the unperturbed energy with respect to the action (n_0). For $n_0=37$ this corresponds to a frequency of $f=9.5$ GHz. This is very close to two prominent prethreshold structures at $f=8.9$ GHz and $f=9.9$ GHz. $f=9.5$ GHz approximately corresponds to a 12-photon transition from $n=37$ to $n=38$ and an 11-photon transition from $n=38$ to $n=39$. We call this condition a "double-resonance condition." At 9.92 GHz we found that it occurs only at $n_0=37$.

The double-resonance criterion can be applied to all n_0. As an example, Fig. 6 shows $P_<(n_0=10,f)$ around the frequency given by the double-resonance criterion, $f=1366$ GHz. There is a pronounced prethreshold structure in the computed data for $f\approx 1380$ GHz. Figure 6 shows that (i) prethreshold structures exist for a wide range of n_0 and (ii) the double-resonance criterion predicts the frequency at which, in general, the most pronounced prethreshold structures can be found (we checked this for several n_0). The latter is somewhat surprising since the n_0+2 level is strongly perturbed at the position of the prethreshold structure.

The name "prethreshold structure" was chosen because these ionization features occur for field strengths where no classical ionization is allowed. Classically the ionization thresholds are sharp [38]. Therefore there is no problem deciding whether a certain ionization feature qualifies as a prethreshold feature or not. For all n_0 that show prethreshold structures (see Fig. 2) we solved the classical SSE equations governed by the Hamiltonian function

$$H(p,z)=p^2/2-1/z+\epsilon z\sin(\omega t), \tag{23}$$

where p and z are classical, canonically conjugate variables. Solving the canonical equations $\dot{z}=\partial H(p,z)/\partial p$ and $\dot{p}=-\partial H(p,z)/\partial z$, we computed the uniquely determined classical critical fields $\mathcal{E}_{\rm cr}(n_0;\omega)$, which mark the onset of classical ionization. These fields are listed as the fourth column in Table I. The classical critical fields can be compared with the field strengths at which prethreshold structure occurs. The prethreshold structures of $n_0=32$, $n_0=34$, and $n_0=45$ are embedded in the main rise of the ionization signal in Fig. 2. For these values of n_0, the anticrossing marking the position of the prethreshold structure is at or slightly above the classical critical fields. However, because of the widths of the prethreshold structures, they extend below the classical critical fields and are therefore clearly seen as prethreshold structures in both the SSE calculations and the experimental data in Fig. 2. All other prethreshold structures occurring in Fig. 2 and summarized in Table I occur *below* the classical critical fields. Since the critical fields $\mathcal{E}_{\rm cr}(n_0;\omega)$ also mark the onset of classical chaos, we expect that the level structure of the one-dimensional hydrogen atom for fields larger than $\mathcal{E}_{\rm cr}(n_0;\omega)$ is very complicated. Conversely, for fields smaller than $\mathcal{E}_{\rm cr}(n_0;\omega)$—i.e., in the prethreshold region—where the classical phase space is dominated by invariant *KAM* lines [3], we expect that the system has well-defined energy levels. This is indeed the case, as Fig. 5 shows, and explains why our method works.

Prethreshold structure also occurs in two-frequency ionization experiments [39] where even double structures with two distinct prethreshold peaks can occur. Using the method of successive rational approximations to the experimental frequency ratio [40] our analytical method, crucially depending on the quasienergy picture, which requires a periodic drive, can be applied even to the adiabatic two-frequency cases.

VII. CONCLUSIONS

Having been much less of a focus than high scaled frequency $(\omega_0>1)$, the low-frequency regime $(\omega_0<1)$ of microwave ionization of hydrogen Rydberg atoms deserves further detailed attention. In this paper we present a complete

classification of prethreshold structures in experimental data by assigning a multiphoton order to each prethreshold structure. We show that a fourth-order perturbation calculation accurately predicts the positions of prethreshold structures. Our analytical and numerical calculations are accurate enough to predict field and frequency combinations where additional prethreshold structures may be found experimentally.

ACKNOWLEDGMENTS

T.C. gratefully acknowledges the support of the Danish Research Council. We are grateful to Peter Koch for providing us with the digitized versions of the experimental microwave ionization data shown in Figs. 1 and 2. This work was supported by NSF Grant No. PHY-9984075.

[1] J. E. Bayfield and P. M. Koch, Phys. Rev. Lett. **33**, 258 (1974).
[2] B. I. Meerson, E. A. Oks, and P. V. Sasarov, JETP Lett. **29**, 72 (1979).
[3] G. Casati, B. V. Chirikov, D. L. Shepelyansky, and I. Guarneri, Phys. Rep. **154**, 77 (1987).
[4] C. H. Cheng and T. F. Gallagher, Phys. Rev. A **61**, 063411 (2000).
[5] K. A. H. van Leeuwen, G. v. Oppen, S. Renwick, J. B. Bowlin, P. M. Koch, R. V. Jensen, O. Rath, D. Richards, and J. G. Leopold, Phys. Rev. Lett. **55**, 2231 (1985).
[6] P. M. Koch and K. A. H. van Leeuwen, Phys. Rep. **255**, 289 (1995).
[7] D. Richards, J. G. Leopold, P. M. Koch, E. J. Galvez, K. A. H. van Leeuwen, L. Moorman, B. E. Sauer, and R. V. Jensen, J. Phys. B **22**, 1307 (1989).
[8] A. Krug and A. Buchleitner, Phys. Rev. A **66**, 053416 (2002).
[9] A. Krug and A. Buchleitner, Comput. Phys. Commun. **147**, 394 (2002).
[10] A. Krug and A. Buchleitner, Phys. Rev. Lett. **86**, 3538 (2001).
[11] P. Fu, T. J. Scholz, J. M. Hettema, and T. F. Gallagher, Phys. Rev. Lett. **64**, 511 (1990).
[12] M. W. Noel, W. M. Griffith, and T. F. Gallagher, Phys. Rev. A **62**, 063401 (2000).
[13] H. P. Breuer, K. Dietz, and M. Holthaus, J. Phys. B **22**, 3187 (1989).
[14] Y. Zhang, M. Ciocca, L. W. He, C. E. Burkhardt, and J. J. Leventhal, Phys. Rev. A **50**, 4608 (1994).
[15] P. M. Koch, E. J. Galvez, and S. A. Zelazny, Physica D **131**, 90 (1999).
[16] Peter Koch was kind enough to send us the digitized data of the Stony Brook hydrogen ionization experiments as published in [6] and used here in Figs. 1 and 2.
[17] P. M. Koch, in *Proceedings of the NATO Advanced Research Workshop on Fundamental Aspects of Quantum Theory*, edited by V. Govini and A. Frigerio (Plenum, New York, 1986), p. 173.
[18] A. K. Dhar, M. A. Nagarajan, F. M. Izrailev, and R. R. Whitehead, J. Phys. B **16**, L17 (1983).
[19] R. Blümel and U. Smilansky, Z. Phys. D: At., Mol. Clusters **6**, 83 (1987).
[20] R. Blümel and U. Smilansky, Phys. Scr. **35**, 15 (1987).
[21] D. Richards, J. Phys. B **20**, 2171 (1987).
[22] A. Buchleitner, D. Delande, and J.-C. Gay, J. Opt. Soc. Am. B **12**, 505 (1995).
[23] A. Buchleitner and D. Delande, Phys. Rev. Lett. **70**, 33 (1993).
[24] http://www.weswulf.org
[25] R. V. Jensen, Phys. Rev. Lett. **49**, 1365 (1982).
[26] G. N. Rockwell, V. F. Hoffman, T. Clausen, and R. Blümel, Phys. Rev. A **65**, 025401 (2002).
[27] E. Hairer, S. P. Norsett, and G. Wanner, *Solving Ordinary Differential Equations I:Nonstiff Problems*, 2nd ed. (Springer, Berlin, 1993).
[28] G. Floquet, Ann. Ecole Norm. Suppl. **12**, 44 (1883).
[29] *Handbook of Mathematical Functions*, edited by M. Abramowitz and I. A. Stegun (National Bureau of Standards, Washington, D. C., 1964).
[30] J. S. Shirley, Phys. Rev. **138**, B979 (1965).
[31] Y. B. Zeldovich, Sov. Phys. JETP **24**, 1006 (1967).
[32] F. Bloch, Z. Phys. **49**, 31 (1928).
[33] H. Friedrich, *Theoretical Atomic Physics* (Springer, Berlin, 1994).
[34] A. Buchleitner and D. Delande, Chaos, Solitons Fractals **5**, 1125 (1995).
[35] S. Yoshida, C. O. Reinhold, P. Kristöfel, and J. Burgdörfer, Phys. Rev. A **62**, 023408 (2000).
[36] S. Yoshida, C. O. Reinhold, P. Kristöfel, J. Burgdörfer, S. Watanabe, and F. B. Dunning, Phys. Rev. A **59**, R4121 (1999).
[37] E. Persson, S. Yoshida, X.-M. Tong, C. O. Reinhold, and J. Burgdörfer, Phys. Rev. A **68**, 063406 (2003).
[38] B. Sundaram and R. V. Jensen, Phys. Rev. A **51**, 4018 (1995).
[39] L. Moorman, E. J. Galvez, B. E. Sauer, A. Mortazawi-M., K. A. H. van Leeuwen, G. v. Oppen, and P. M. Koch, Phys. Rev. Lett. **61**, 771 (1988).
[40] R. Blümel, G. Jaeckel, and U. Smilansky, Phys. Rev. A **39**, 450 (1989).